

Article

Mechanism and Prevention of Rock Burst in a Wide Coal Pillar under the Superposition of Dynamic and Static Loads

Bangyou Jiang ¹, Yanan Xu ¹, Wenshuai Li ^{2,*}, Shitan Gu ^{1,*} and Mingjun Ding ¹

¹ College of Energy and Mining Engineering, Shandong University of Science and Technology, Qingdao 266590, China; jiangbangyou123@163.com (B.J.); 17863981815@163.com (Y.X.); dingmj123@163.com (M.D.)

² College of Civil Engineering and Architecture, Shandong University of Science and Technology, Qingdao 266590, China

* Correspondence: lwsnote@163.com (W.L.); chinasdgst@163.com (S.G.)

Abstract: To address the frequent occurrence of rock burst disasters in areas with wide coal pillars during mining in the western mining area of China, the wide coal pillar area of the Tingnan coal mine in Shanxi Province was used as the research background. Theoretical analysis, numerical simulation, and field tests were used to establish the mechanical criterion and the energy criterion for the dynamic instability of wide coal pillars. The process and mechanism of wide coal pillar dynamic instability under dynamic and static load disturbances were revealed, and a wide coal pillar rock burst prevention and control scheme was proposed. The results indicated that when the load above a coal pillar reached the stress failure index and the energy failure index was met, the coal pillar reached the critical conditions for rock burst. With increasing static load, the stress, energy, and range of the plastic zone all showed increasing trends on both sides of the coal pillar. Under a given dynamic load, the stress and plastic zone range of the coal pillar significantly increased compared to those without a dynamic load. Under a given static load, the greater the dynamic load, the more likely the coal pillar was to undergo dynamic instability. The evolution of coal pillar dynamic instability was divided into three stages: energy accumulation, local instability, and dynamic instability. When the critical stress and energy conditions for coal pillar dynamic instability are exceeded, rock burst will occur. To reduce the static and dynamic loads of coal pillars, a rock burst prevention and control scheme of energy release and load reduction was proposed and applied onsite. The monitoring results showed that this control plan effectively reduced the stress of the coal pillar and the dynamic load generated by the fracture of the overlying rock layer, indicating safe mining in this area of wide coal pillars.

Keywords: wide coal pillar; superimposition of dynamic and static loads; rock burst; prevention and control



Citation: Jiang, B.; Xu, Y.; Li, W.; Gu, S.; Ding, M. Mechanism and Prevention of Rock Burst in a Wide Coal Pillar under the Superposition of Dynamic and Static Loads. *Processes* **2024**, *12*, 1634. <https://doi.org/10.3390/pr12081634>

Academic Editors: Yuanyuan Pu, Sitao Zhu and Xinglong Zhao

Received: 28 June 2024

Revised: 23 July 2024

Accepted: 24 July 2024

Published: 3 August 2024



Copyright: © 2024 by the authors. Licensee MDPI, Basel, Switzerland. This article is an open access article distributed under the terms and conditions of the Creative Commons Attribution (CC BY) license (<https://creativecommons.org/licenses/by/4.0/>).

1. Introduction

With long-term, large-scale, and high-intensity mining, the frequency and destruction intensity of coal mine rock burst disasters in China are increasing [1–5]. To improve the ventilation and auxiliary transportation required for high-yield and high-efficiency mining, working faces in western mining areas in China typically adopt a layout of double roadways and coal pillars with widths of 20–40 m. At present, multiple coal mines in the western mining areas have experienced rock burst accidents due to the retention of coal pillars with inappropriate sectional dimensions [6], posing a serious threat to the safety of coal mine production. The retention of coal pillars with inappropriate sectional dimensions has become an important factor influencing the occurrence of rock burst. For example, under long-term high static loads, coal pillars are prone to damage. Additionally, dynamic loads induced by fractures in the overlying strata further exacerbate the damage degree of coal pillars. Under the combined action of the above two types of loads, coal pillars are prone to impact damage [7]. Therefore, conducting research on the mechanism and prevention

of wide coal pillar-controlled rock burst under combined dynamic and static loading is considerably important for achieving the safe and efficient production of coal mines.

Many scholars have conducted extensive research on the mechanism of rock burst induced by coal pillars and rock burst prevention and control methods [8–12]. Yu et al. [13] studied the stress distribution of coal pillars under repeated mining influence, obtaining the stress distribution characteristics of coal pillars after primary and secondary mining. Zhang et al. [14] theoretically calculated the stress state of coal pillars after roof failure. Wang [15] analyzed the characteristics of roof fracture along a goaf and the stress characteristics of coal pillars. Zhang et al. [16] suggested that structural control measures such as roof prefracture should be adopted for the prevention and control of rock burst in coal–rock masses.

The mechanism by which the overlying strata structure affects the load on coal pillars from a static perspective after the overlying rock layer breaks has been investigated. However, under the influence of mining activities, the movement of the overlying strata significantly increases the static load on the coal pillars, and the dynamic load induced by rock rupture also strongly disturbs the coal pillars [17–19]. In this case, wide coal pillars are often subjected to combined dynamic and static loading. Dou et al. [20] established a comprehensive early warning method for rock burst based on the principle of dynamic and static load superposition. They proposed a method to prevent rock burst by reducing the static load on a coal–rock mass, mitigating the dynamic load induced by mine-induced earthquakes, and increasing the critical stress threshold [18,21,22].

Many scholars have conducted in-depth research on the failure of coal pillars under static or dynamic loading and have obtained many important findings. However, due to the complexity arising from the superposition of dynamic and static loads, there has been relatively little research on the failure of wide coal pillars under such combined disturbances. Therefore, taking the wide coal pillars in the Tingnan coal mine in the Binchang mining area as the research objects, the critical conditions for dynamic instability of wide coal pillars were studied. This study aimed to determine the mechanism of coal pillar dynamic instability under the influence of both dynamic and static loads. Based on these findings, a technique for preventing and controlling rock burst induced by the instability of wide coal pillars was proposed, thereby providing theoretical support and practical experience for the safe production of coal mines under similar conditions.

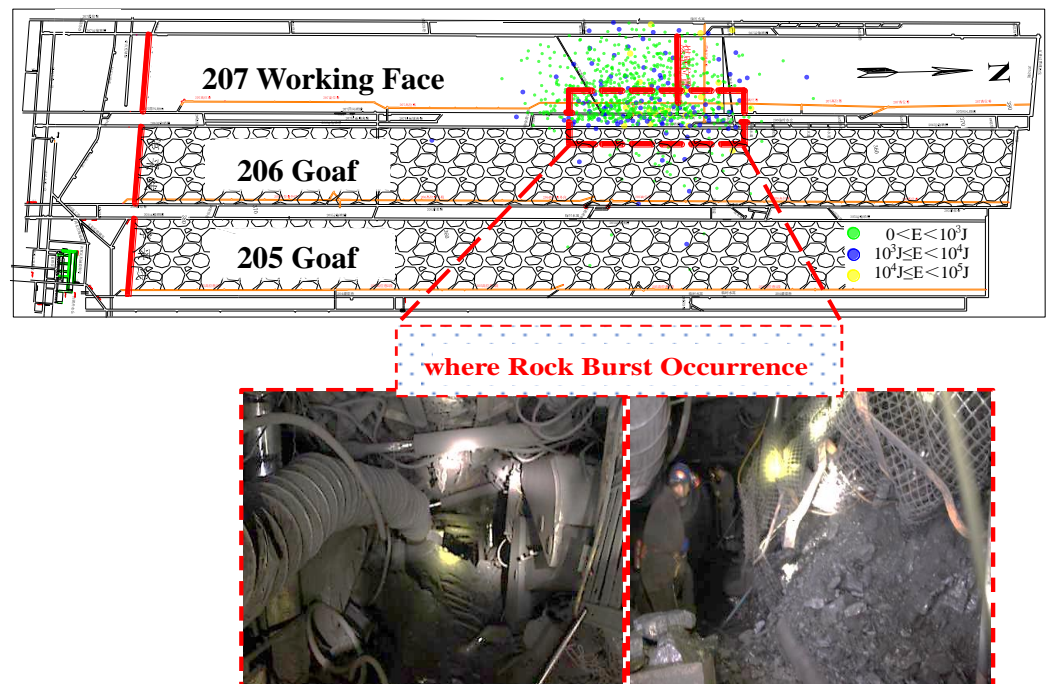
2. Engineering Background

The Tingnan coal mine is located in Xianyang, Shanxi Province, China, as shown in Figure 1a. The 207 working face of the Tingnan coal mine is located in the eastern part of the second panel. The western side is a solid coal area, while the eastern side is the goaf of the 205 and 206 working faces, with a 30 m wide coal pillar reserved between adjacent working faces. The buried depth of the working face ranges from 462 m to 714 m. The average thickness of the coal seam is approximately 15.63 m, with a dip angle ranging from 0° to 7°. Fully mechanized top coal caving mining technology is adopted here, with a cutting height of 3.5 m, and the mining speed of the working face is 4.0–4.8 m/d. Within 100 m above the coal seam, there are multiple layers of thick hard strata, such as sandstone (12.7 m of coarse grained sandstone with gravel and 17.1 m of coarse-grained sandstone), as shown in Figure 2.

When the No. 207 working face was mined up to 739.6 m, a high-energy microseismic event with 3.4×10^5 J was detected 65 m ahead and 5.7 m to the west in the transportation roadway (along the goaf). Moreover, within a range of approximately 35 to 58 m ahead of the working face, collapse was detected in some areas near the coal pillar side, and severe deformation and convergence of the roadway were observed, as shown in Figure 1b.



(a) Location of the Tingnan coal mine



(b) Location of rock burst occurrence

Figure 1. The area where a rock burst occurred in the 207 working face in the Tingnan coal mine.

NO.	Columnar	Lithology	Layer Thickness (m)
1		Medium-grained sandstone	66.0
2		Fine-grained sandstone	12.2
3		Fine-grained sandstone	12.9
4		Coarse-grained sandstone	31.4
5		Fine-grained sandstone	17.0
6		Sandy Mudstone	21.3
7		Coarse-grained sandstone	17.1
8		Slity Mudstone	7.40
9		Coarse grained sandstone with gravel	12.7
10		Sandy Mudstone	14.2
11		Coarse grained sandstone with gravel	2.50
12		Slity Mudstone	14.0
13		Coarse-grained sandstone	6.20
14		Slity Mudstone	33.5
15		Sandy Mudstone	1.37
16		No.4 Coal seam	15.6
17		Sandy Mudstone	20.2

Figure 2. Borehole stratigraphy of 207 working face in the Tingnan coal mine.

3. Critical Failure Conditions of Wide Coal Pillars under the Combined Effect of Dynamic and Static Loading

3.1. Stress Conditions

From a stress perspective, the static load exerted on a coal pillar primarily comes from the weight of the overlying strata and the load transferred from the strata above the goaf. Additionally, factors such as the strength of the coal itself and the intensity of dynamic load disturbances also need to be considered. When the stress exerted on the coal pillar reaches 1.5 times its comprehensive compressive strength, the coal pillar will be in a critical state of instability. The critical condition for the failure of the coal pillar is

$$I_d = \frac{\lambda\sigma_m}{\bar{\mu}[\sigma_c]} > 1.5 \quad (1)$$

where I_d is the stress failure index of the coal pillar; λ is the dynamic load disturbance coefficient, which is the ratio of the sum of the in situ stress and the dynamic load disturbance stress to the in situ stress; σ_m is the average stress on the coal pillar (MPa), which can be calculated from the transferred load of the overlying strata and the weight of the strata [23]; $[\sigma_c]$ is the uniaxial compressive strength of the coal (MPa); and $\bar{\mu}$ is the average comprehensive compressive coefficient of the coal and can be expressed as [24]

$$\bar{\mu} = \frac{L_m - 2x_1}{L_m} \mu_{\max} + \frac{2x_1}{L_m} \mu_{\min} \quad (2)$$

where L_m is the coal pillar width; x_1 is the range of the plastic zone on the side of the coal pillar; μ_{\max} in the elastic region of the coal is taken to be 3 to 5; and μ_{\min} in the plastic or fractured zone of the coal wall is approximately equal to 1.

3.2. Energy Conditions

According to the theory of elastic mechanics, the elastic energy stored per unit volume within the coal–rock mass can be expressed as

$$E_e = \frac{\sigma_1^2 + \sigma_2^2 + \sigma_3^2 - 2\mu(\sigma_1\sigma_2 + \sigma_1\sigma_3 + \sigma_2\sigma_3)}{2E} \quad (3)$$

where σ_1 , σ_2 , and σ_3 are the maximum principal stress, intermediate principal stress, and minimum principal stress (MPa), respectively; E is the elastic modulus of the coal and rock mass (MPa); and μ is Poisson's ratio.

The shear failure of the coal and rock mass satisfies the Mohr–Coulomb criterion:

$$\sigma_1 = \frac{1 + \sin \varphi}{1 - \sin \varphi} \sigma_3 + \frac{2c \cos \varphi}{1 - \sin \varphi} \quad (4)$$

where φ is the internal friction angle ($^\circ$) and c is the cohesion (MPa).

The dimensions of the coal pillar in the length direction are much larger than those in the other two directions, which constitutes a plane strain problem:

$$\sigma_2 = \mu(\sigma_1 + \sigma_3) \quad (5)$$

The critical energy of the coal pillar failure is

$$E_s = \frac{A\sigma_3^2 + 2B\sigma_3 + 2c^2 \cos^2 \varphi (1 - \mu^2)}{E(1 - \sin \varphi)^2} \quad (6)$$

$$A = -2\mu^2 + \mu(\sin^2 \varphi - 1) + 1 + \sin^2 \varphi \quad (7)$$

$$B = c \cos \varphi [-2\mu^2 + \mu(\sin \varphi - 1) + 1 + \sin \varphi] \quad (8)$$

When the sum of the elastic energy E_e stored in the coal pillar and the dynamic disturbance energy E_d exceeds the critical energy E_s , the coal mass will undergo dynamic instability. Thus, the energy condition for the dynamic instability of the coal pillar is [25]

$$I_s = \frac{E_s}{E_e + E_d} < 1 \quad (9)$$

where I_s is the energy failure index of the coal pillar.

When the load above the coal pillar reaches the stress condition for coal pillar failure and the sum of the elastic energy stored in the coal pillar and the dynamic disturbance energy exceeds the critical energy, dynamic instability of the coal pillar will occur.

4. The Mechanical Response and Dynamic Instability Mechanism of Coal Pillars under Dynamic Load Disturbance

4.1. Model Establishment

To study the mechanical response characteristics and dynamic instability mechanism of wide coal pillars under the influence of dynamic and static loads, a roof–coal pillar model was established using FLAC^{3D} (version 6.0). The model dimensions were 50 m (length) \times 50 m (width) \times 85 m (height). The boundary conditions of the model were as follows: horizontal and vertical constraints were applied to the side and bottom of the model, respectively, and a vertical stress was applied at the top of the model to simulate the weight of the overlying strata, as shown in Figure 3. Table 1 lists the basic mechanical parameters of the coal and rock mass.

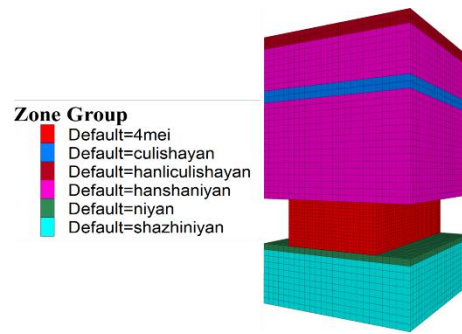


Figure 3. Numerical calculation model of roof–coal pillar.

Table 1. Mechanical parameters of the coal and rock mass for simulation.

Rock Types	Bulk Modulus (GPa)	Shear Modulus (GPa)	Tensile Strength (MPa)	Cohesion (MPa)	Friction Angle (°)
Coarse-grained sandstone	13.24	13.24	13.24	13.24	13.24
Medium-grained sandstone	12.26	12.26	12.26	12.26	12.26
Fine-grained sandstone	7.23	7.23	7.23	7.23	7.23
Coarse-grained sandstone	8.12	8.12	8.12	8.12	8.12
Sandy mudstone	3.12	3.12	3.12	3.12	3.12
Coarse grained sandstone with gravel	10.23	10.23	10.23	10.23	10.23
Silty mudstone	3.12	3.12	3.12	3.12	3.12
No.4 coal seam	1.83	1.83	1.83	1.83	1.83
Mudstone	3.02	3.02	3.02	3.02	3.02

4.2. Simulation Scheme

To determine the position and magnitude of the dynamic load applied during a simulation, Table 2 presents the statistical results of the maximum energy of microseismic events during mining from August to October 2017 and from March to April 2018.

Table 2. Statistical results of the maximum energy of microseismic events during mining in the Tingnan coal mine.

Time	Advance Distance (m)	Maximum Energy (J)	The Central Location
2017.08.15–08.31	70	3.21×10^3	33.6 m above coal seam
2017.09.01–09.30	121	6.43×10^4	65.3 m above coal seam
2017.10.01–10.31	66	3.42×10^4	40.2 m above coal seam
2018.03.01–03.31	96	4.02×10^4	76.2 m above coal seam
2018.04.01–04.21	116	3.40×10^5	85.5 m above coal seam

As shown in Table 2, the source of microseismic event with maximum energy was located 85.5 m above the coal seam. Therefore, dynamic load waves were applied 85 m above the coal seam to simulate the dynamic response of coal pillars.

Based on the dynamic load range at the source location, the normal stress generated by mining-induced seismic events with energies above 10^4 J generally ranged from 5.0 to 32.7 MPa, while the shear stress typically ranged from 2.88 to 18.8 MPa [26]. According to Table 2, the maximum energy of the microseismic event reached 3.40×10^5 J. Taking these factors into consideration, the dynamic load adopted in the simulation was set to 5~20 MPa.

To investigate the mechanical response of wide coal pillars under dynamic load, three schemes were selected: (1) determining the mechanical response of the coal pillars under different static loads without a dynamic load applied; (2) determining the mechanical response of the coal pillars under different static loads and a given dynamic load; and

(3) determining the mechanical response of the coal pillars under different dynamic loads and a given static load.

4.3. Mechanical Response of Wide Coal Pillars under Combined Dynamic and Static Loads

(1) Mechanical response of the coal pillar under different initial static loads without a dynamic load applied

According to the burial depth of the working face, the load above the model was determined to be 9.1 MPa. To study the stress, energy accumulation, and plastic zone distribution of the coal pillars under different static loads, four static loads (5 MPa, 8 MPa, 12 MPa, and 15 MPa) were selected for analysis. The mechanical response and curves of the coal pillars are shown in Figures 4 and 5.

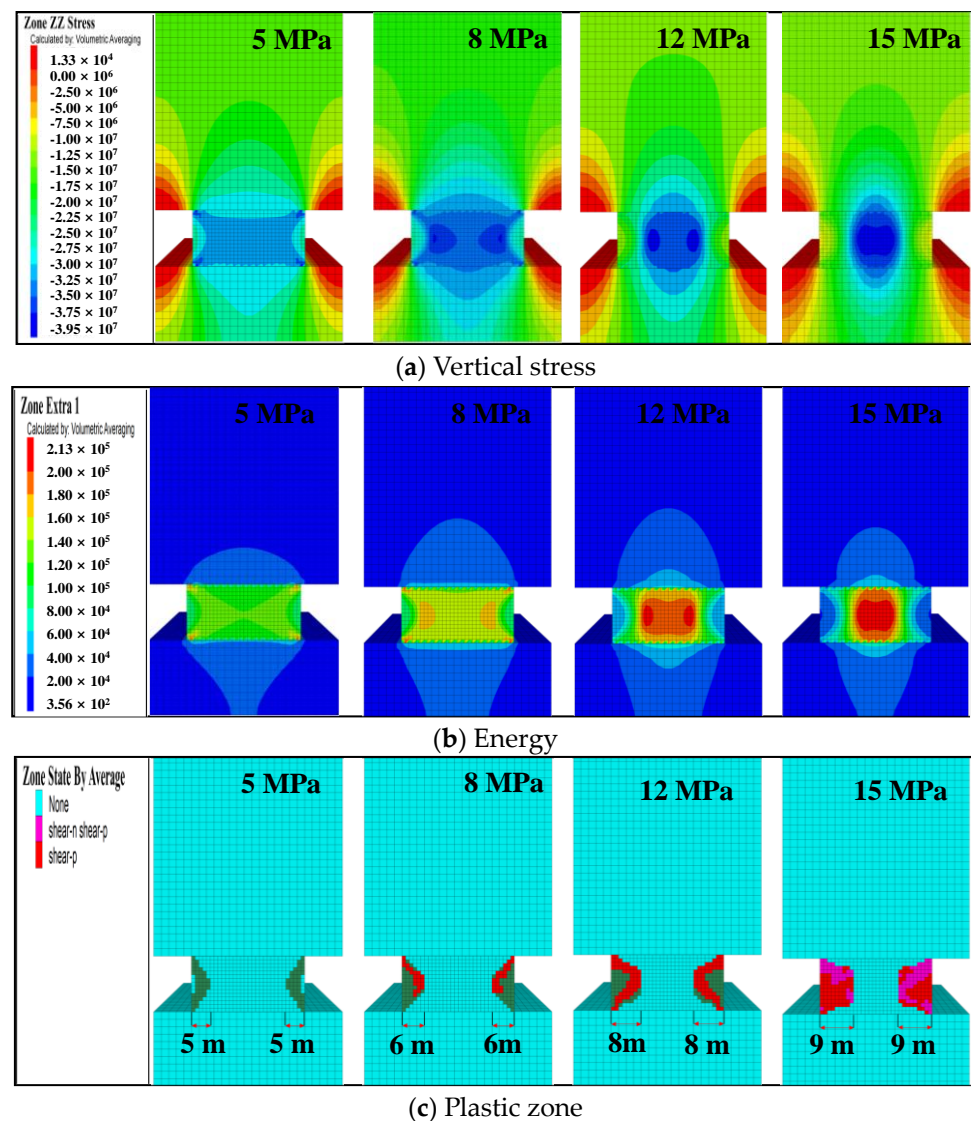


Figure 4. Mechanical response contour maps of coal pillar under different static loads (5 MPa, 8 MPa, 12 MPa, and 15 MPa).

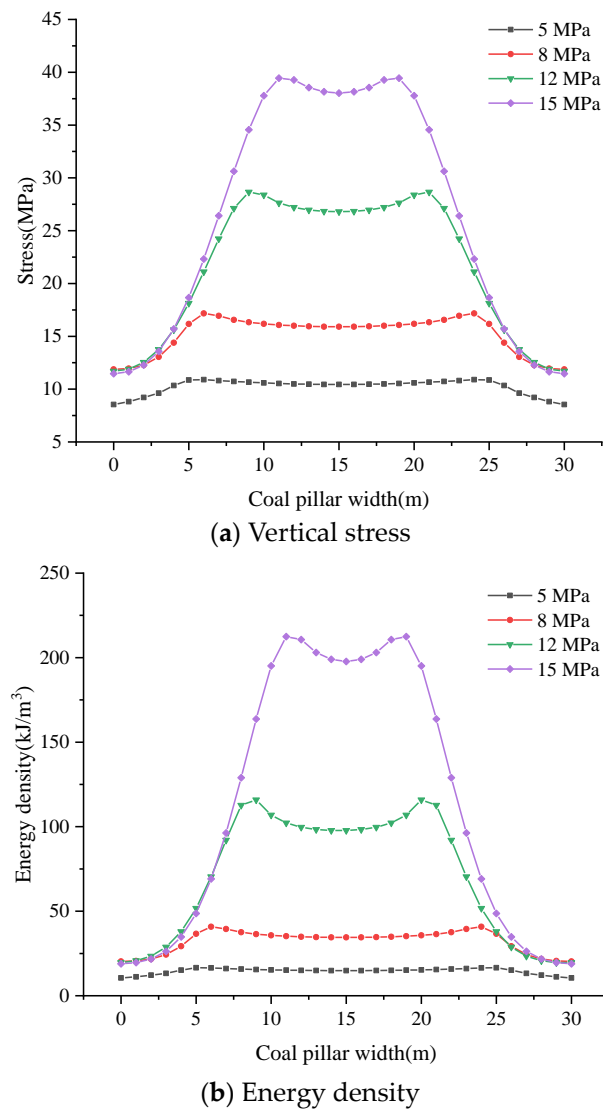


Figure 5. Mechanical response curves of coal pillar under different static loads (5 MPa, 8 MPa, 12 MPa, and 15 MPa).

As shown in Figures 4 and 5, without considering a dynamic load, as the static load increases, the vertical stress, energy accumulation, and extent of the plastic zone above the coal pillar all increase. When the static load is 8 MPa, plastic failure zones 6 m wide form on both sides of the coal pillar (as shown in Figure 4c), but the overall stability of the coal pillar is maintained. As the static load further increases, the stress on the coal pillar continues to rise, and the plastic zones also gradually expand on both sides of the coal pillar. When the static load increases from 5 MPa to 15 MPa, the peak vertical stress above the coal pillar increases from 11.1 MPa to 39.5 MPa, with a rate of increase of approximately 256%; the peak energy density increases from 27.0 kJ/m³ to 206.5 kJ/m³, with a rate of increase of approximately 665%; and the plastic zone extends from 5 m to 9 m, with an increase of approximately 80%.

(2) Mechanical response of coal pillar under a given dynamic load (10 MPa) and different static loads

Under the condition of four tested static loads (5 MPa, 8 MPa, 12 MPa, and 15 MPa), a dynamic load of 10 MPa was applied. Figures 6 and 7 present the mechanical response contour maps and curves of the coal pillars.

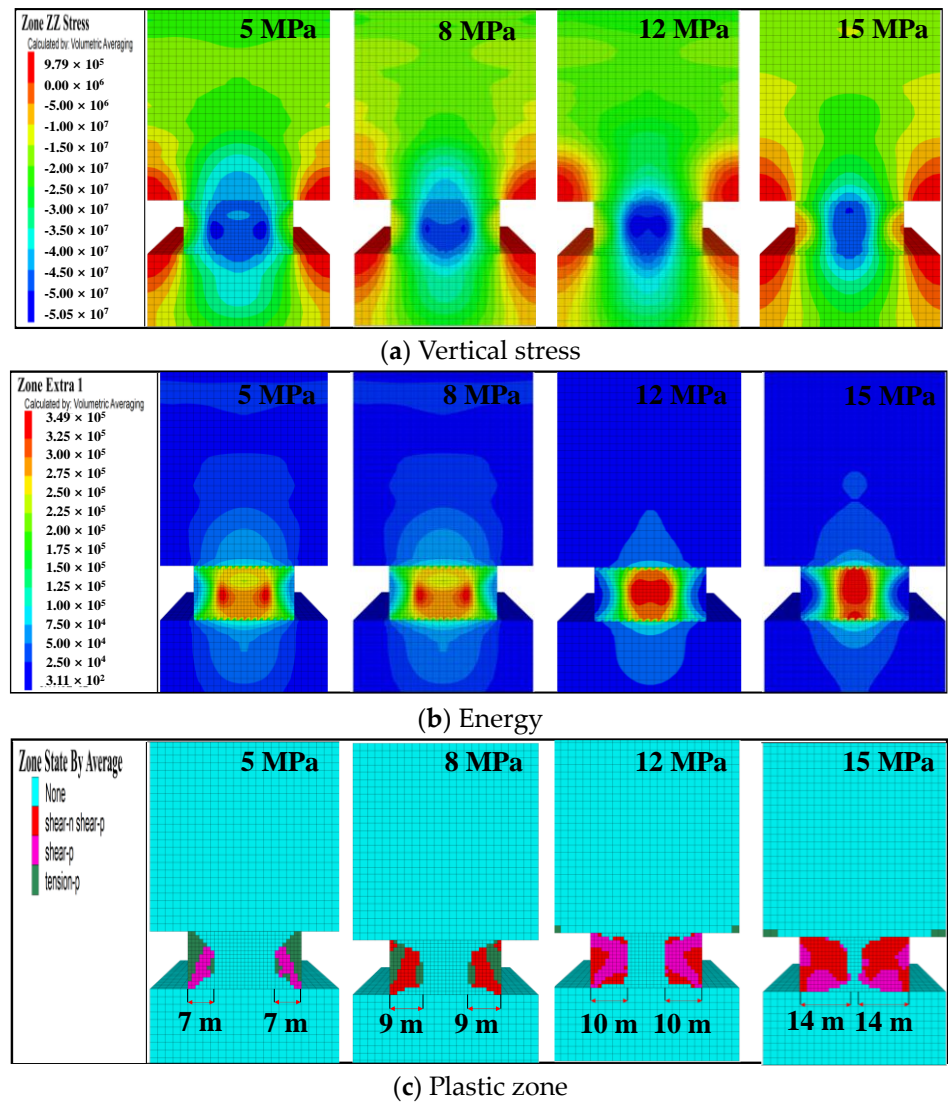


Figure 6. Mechanical response contour maps of coal pillar under a given dynamic load (10 MPa) and different static loads (5 MPa, 8 MPa, 12 MPa, and 15 MPa).

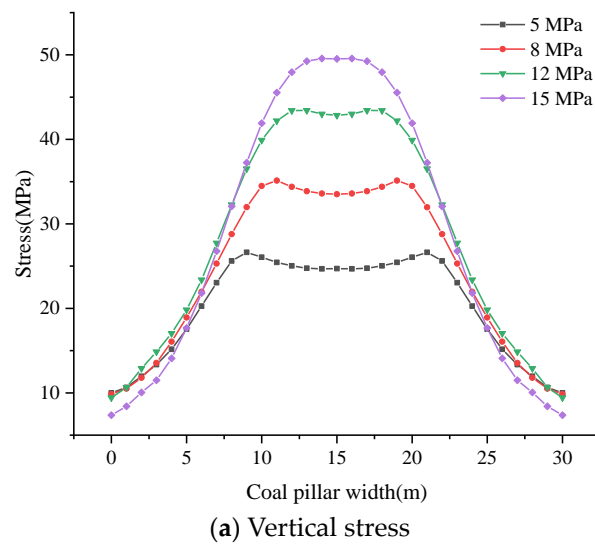


Figure 7. Cont.

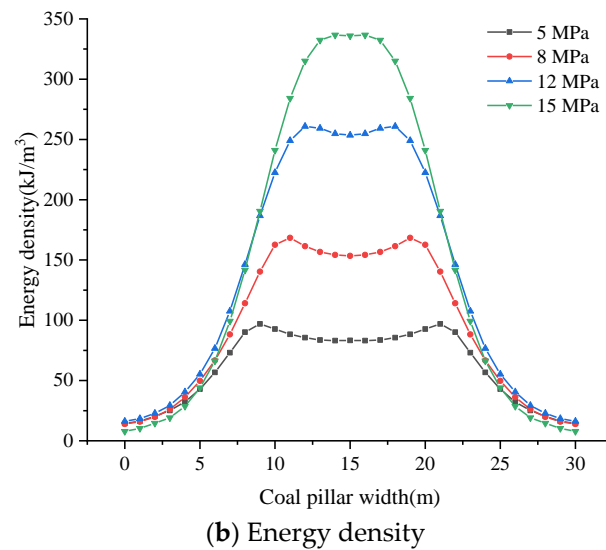


Figure 7. Mechanical response curves of coal pillar under given dynamic load (10 MPa) and different static loads (5 MPa, 8 MPa, 12 MPa, and 15 MPa).

As shown in Figures 6 and 7, when applying the dynamic load, the vertical stress above the coal pillar significantly increases compared to the condition without the dynamic load, and the extent of the plastic zone also further expands. For instance, under a static load of 12 MPa, after applying dynamic loads, the peak stress increases by approximately 59.3%, and the plastic zone extends from 8 m before applying dynamic load to 10 m. Additionally, when the static load is 15 MPa, the elastic zone of the coal pillar is only 2 m, with a core zone rate of only 6.67%. Previous research has indicated that when the core zone rate is less than 11.92%, the coal pillar is highly likely to undergo catastrophic instability and failure [26].

(3) Mechanical response of coal pillar under a given static load (9 MPa) and different dynamic loads

Under a static load of 9 MPa, different dynamic loads (5 MPa, 10 MPa, 15 MPa, and 20 MPa) were applied. The specific simulation results are shown in Figures 8 and 9.

Figures 8 and 9 show that under a given static load, as the dynamic load increases, the stress, energy accumulation, and plastic zone of the coal pillar all increase. When the dynamic load increases from 5 MPa to 20 MPa, the peak vertical stress above the coal pillar increases from 22.7 MPa to 70.9 MPa, with a rate of increase of approximately 212%, and the peak energy density increases from 56.3 kJ/m³ to 438.5 kJ/m³, with a rate of increase of approximately 679%. Meanwhile, the plastic zone extends from 7 m to 30 m, with a rate of increase of approximately 329%.

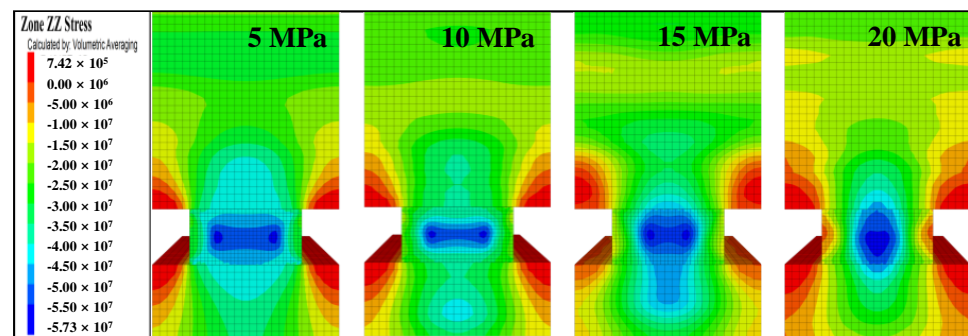


Figure 8. Cont.

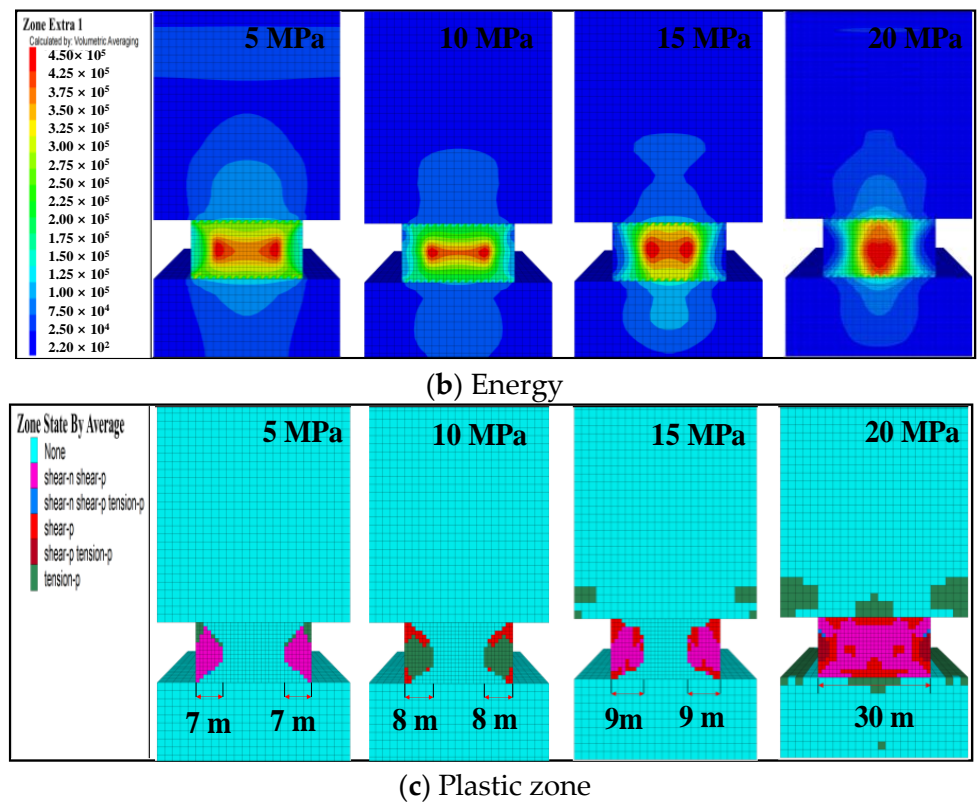


Figure 8. Mechanical response contour maps of coal pillar under a given static load (9 MPa) and different dynamic loads (5 MPa, 10 MPa, 15 MPa, and 20 MPa).

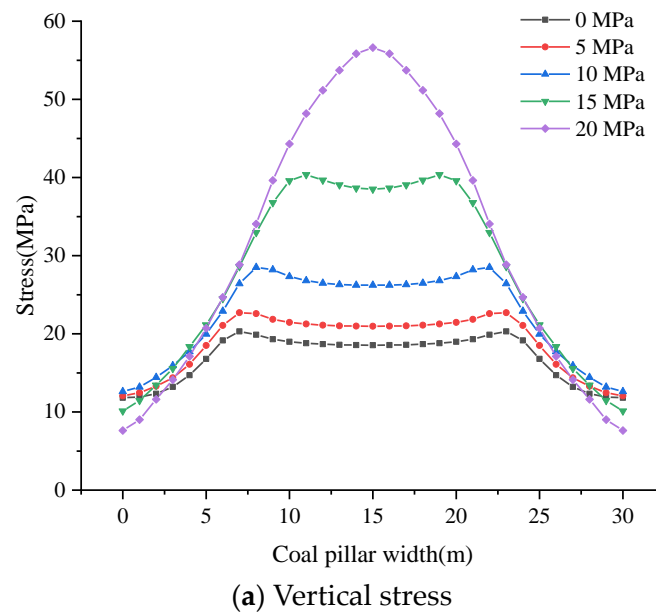


Figure 9. Cont.

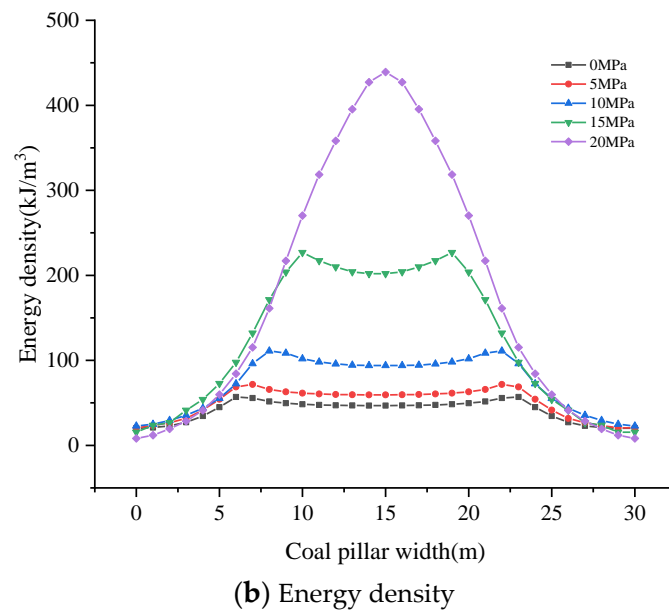


Figure 9. Mechanical response curves of coal pillar under a given static load (9 MPa) and different dynamic loads (5 MPa, 10 MPa, 15 MPa, and 20 MPa).

4.4. Critical Conditions of Dynamic Instability of Wide Coal Pillars under the Superposition of Dynamic and Static Loads

(1) Critical failure analysis of coal pillar under a given dynamic load and different static loads

By substituting the numerical simulation results into the stress failure condition and energy failure condition, the stress failure index (I_d) and energy failure index (I_s) of the coal pillar under given dynamic load and different static loads can be obtained.

Figure 10 presents the stress failure index of coal pillars under given a dynamic load (10 MPa) and different static loads, along with the corresponding critical value. It can be observed that I_d increases with increasing static load. When the static load is below 12 MPa, I_d is lower than the critical value, indicating that the coal pillar has not yet failed. However, when the static load exceeds 12 MPa, I_d surpasses the critical value for coal pillar failure, indicating that the coal pillar has reached the failure condition.

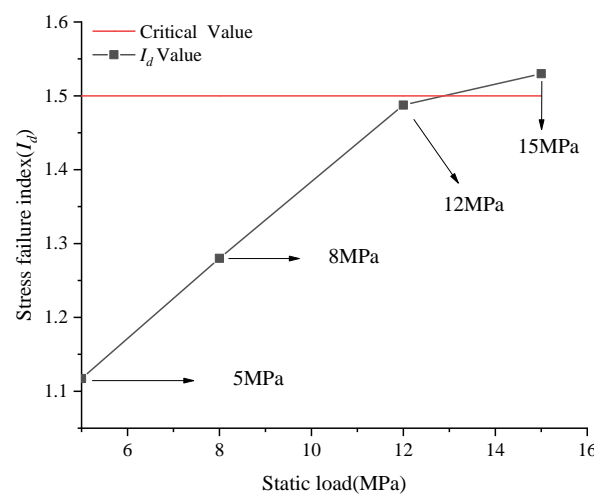


Figure 10. Stress failure index of coal pillars under a given dynamic load (10 MPa) and different static loads (5 MPa, 8 MPa, 12 MPa, and 15 MPa).

Furthermore, Figure 11 illustrates the energy failure index of coal pillars under a given dynamic load (10 MPa) and different static loads, along with the corresponding critical

value. Under the given dynamic load, when the static load is below 12 MPa, the energy failure index of the coal pillar exceeds the critical value. This suggests that the coal pillar has not reached the energy condition for dynamic instability. However, when the static load is 15 MPa, the critical energy condition for dynamic instability is met, indicating that the coal pillar will experience dynamic instability.

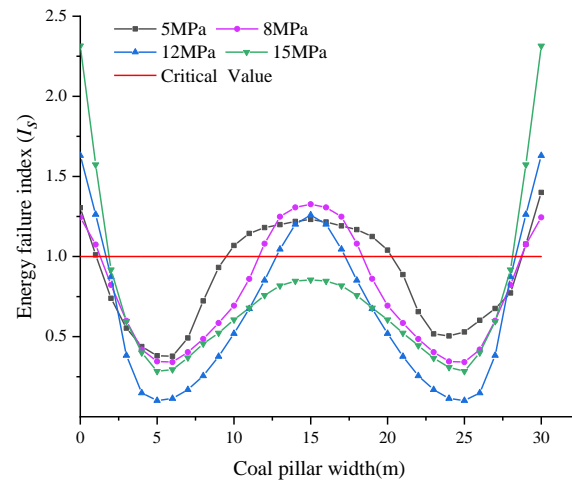


Figure 11. Energy failure index of the coal pillar under a given dynamic load (10 MPa) and different static loads (5 MPa, 8 MPa, 12 MPa, and 15 MPa).

Based on the stress failure index and energy failure index results of the coal pillars, under the same dynamic load, whether a coal pillar experiences dynamic instability is closely related to the magnitude of the static load. When the static load applied to the coal pillar is relatively low, the likelihood of dynamic instability is minimal. However, when the static load reaches a certain level, the combined effect of the dynamic load can easily reach the critical conditions for dynamic instability.

(2) Critical failure analysis of coal pillar failure under a given static load and different dynamic loads

According to the numerical simulation results and the stress and energy conditions for coal pillar failure, the I_d and I_s of coal pillars under a given static load and different dynamic loads can be obtained.

Figure 12 presents the stress failure index under a given static load (9 MPa) and different dynamic loads, along with the corresponding critical value. Figure 12 shows that I_d increases with increasing dynamic load. When the dynamic load is less than 15 MPa, I_d is lower than the critical value, indicating that the coal pillar has not yet failed. However, when the dynamic load reaches 20 MPa, I_d surpasses the critical value for coal pillar failure, indicating that the coal pillar will reach the failure condition.

Figure 13 shows the energy failure index under different dynamic loads with a given static load of 9 MPa, and the critical value is also indicated. As shown in Figure 13, under the given static load, when the dynamic load is less than 15 MPa, the energy failure index of coal pillar is greater than the critical value in most areas, indicating that the coal pillar does not meet the energy conditions for dynamic instability. However, when the dynamic load is 20 MPa, the critical energy for coal pillar dynamic instability is satisfied, resulting in coal pillar dynamic instability.

According to the stress failure index and energy failure index results of the coal pillars, under the same static load, whether the coal pillar undergoes dynamic instability is closely related to the value of the dynamic load. When the dynamic load induced by the breaking of the overlying rock strata is relatively low, the coal pillar generally does not experience dynamic instability and exhibits only an increase in stress. However, when the dynamic load exceeds its critical value, the coal pillar is highly susceptible to dynamic instability due to the combined effect of dynamic and static loads.

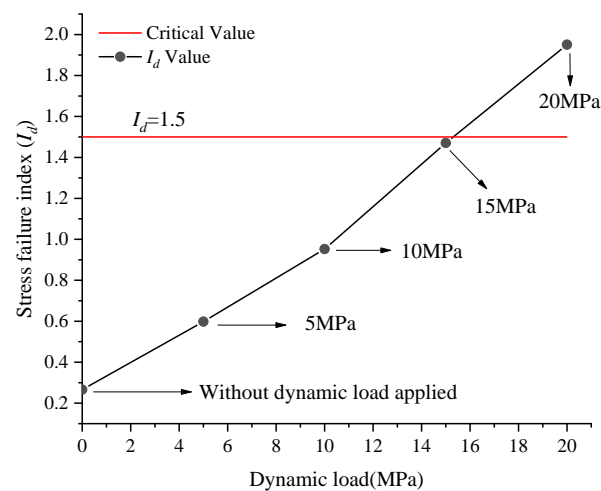


Figure 12. Stress failure index of coal pillars under a given static load (9 MPa) and different dynamic loads (5 MPa, 10 MPa, 15 MPa, and 20 MPa).

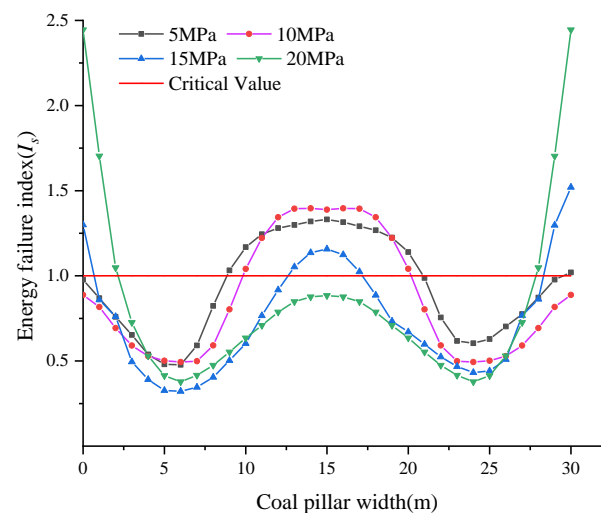


Figure 13. Energy failure index of coal pillars under a given static load (9 MPa) and different dynamic loads (5 MPa, 10 MPa, 15 MPa, and 20 MPa).

4.5. Dynamic Instability Mechanism of Wide Coal Pillars under Superimposed Disturbance from Dynamic and Static Loads

To analyze the dynamic instability mechanism of coal pillars under dynamic and static loads, Figure 14 shows the mechanical response of coal pillars before and after the dynamic load is applied. The following observations were made from this figure: (1) Before the working face is mined, the coal and rock mass are not affected by mining activities, and a coal pillar bears only a static load, resulting in a low probability of dynamic instability. (2) As mining progresses, the extraction space below the roof strata gradually increases. When the roof strata reach their ultimate tensile strength, the roof breaks, releasing elastic energy and forming impact stress waves. These stress waves propagate to the coal pillar, causing the coal pillar, which was initially under a static load, to be subjected to the combined effect of dynamic and static loads. Under a lower dynamic load, the stress waves attenuate to some extent during propagation, having a minor impact on the coal pillar and only increasing its stress level. However, under a higher dynamic load, the combination of the dynamic and static loads can easily exceed the ultimate bearing capacity of the coal pillar, leading to dynamic failure of the coal pillar and resulting in rock burst.

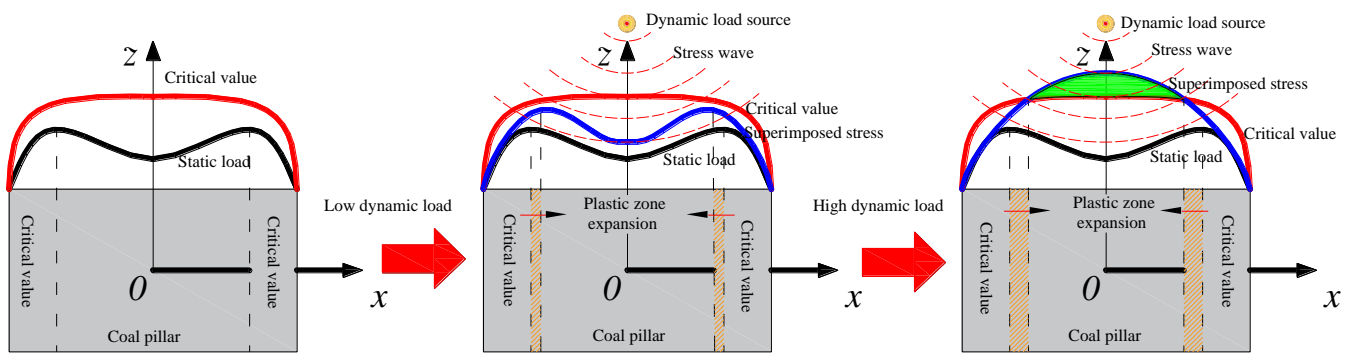
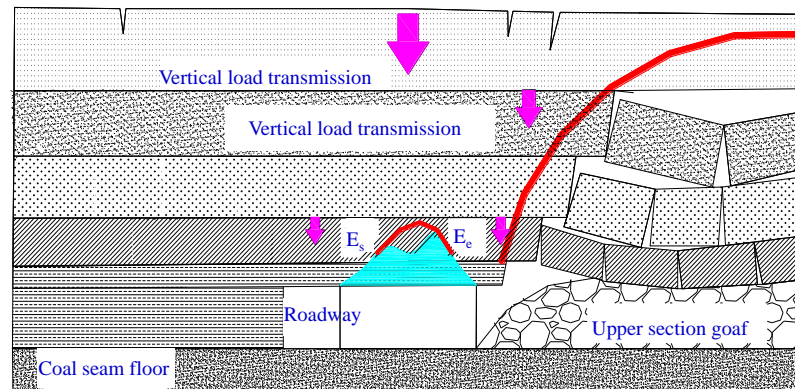
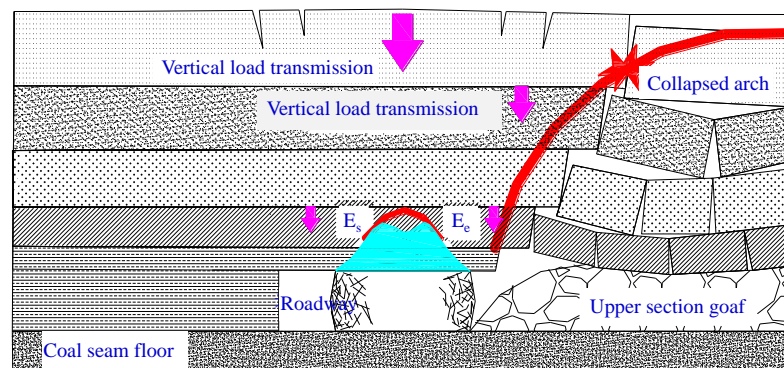


Figure 14. Mechanical response of a coal pillar before and after dynamic loads are applied.

Combining the criteria for coal pillar dynamic instability and the superposition of dynamic and static loads on a coal pillar, the evolution of coal pillar dynamic instability was divided into three stages, the energy accumulation stage, local instability stage and dynamic instability stage, as shown in Figure 15. In the energy accumulation stage, the coal pillar bears a certain static load influenced by the gravity of the overlying strata. As mining advances, the overlying strata break, further increasing the load applied on the coal pillar and leading to energy accumulation. In the local instability stage, the overlying strata break and generate instantaneous dynamic load. Under the combined effects of dynamic and static loads, the ultimate failure strength of the coal mass increases and plastic failure begins to occur at the sides of the coal pillar. In the dynamic instability stage, the energy within the coal pillar continues to accumulate under the effect of dynamic loads. The wide coal pillar rapidly exceeds its ultimate bearing capacity. When the critical conditions of stress and energy for dynamic instability of the coal pillar are surpassed, rock burst occurs.

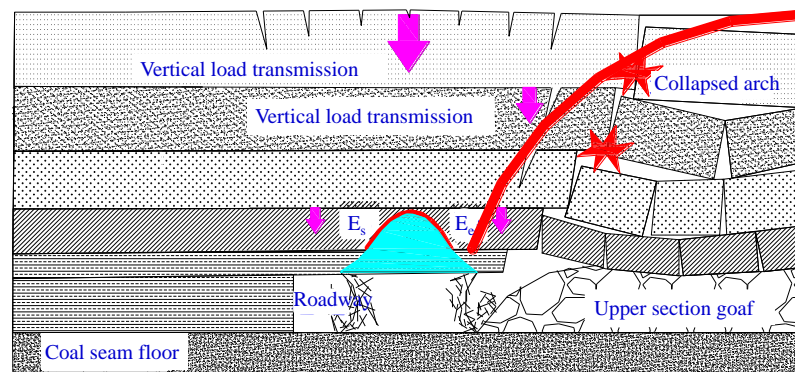


(a) Energy accumulation stage



(b) Local instability stage

Figure 15. Cont.



(c) Dynamic instability stage

Figure 15. Evolution process of coal pillar dynamic instability.

5. Prevention and Control Plan of Rock Burst Induced by Wide Coal Pillars

At the Tingnan coal mine, wide coal pillars were reserved between some working faces, with multiple layers of hard roof strata above the coal seam. During mining, wide coal pillars are prone to stress concentration. Under the disturbance of dynamic load from the breakage of the overlying strata, rock burst is easily induced. Based on the above analysis, taking the 3409 working face of the Tingnan coal mine as an example, a prevention and control plan for mining through the wide coal pillar area was proposed and applied onsite. The 3409 working face mainly contained the No. 4 coal seam, which had a thickness of approximately 8.0 to 18.58 m. A coal pillar with a width of 30 m was preserved between the 3409 working face and the adjacent 3407 goaf. The depth of this region ranged from approximately 470 to 710 m, as shown in Figure 16. According to the borehole stratigraphic diagram, multiple layers of hard and thick roof strata were present above the coal seam.

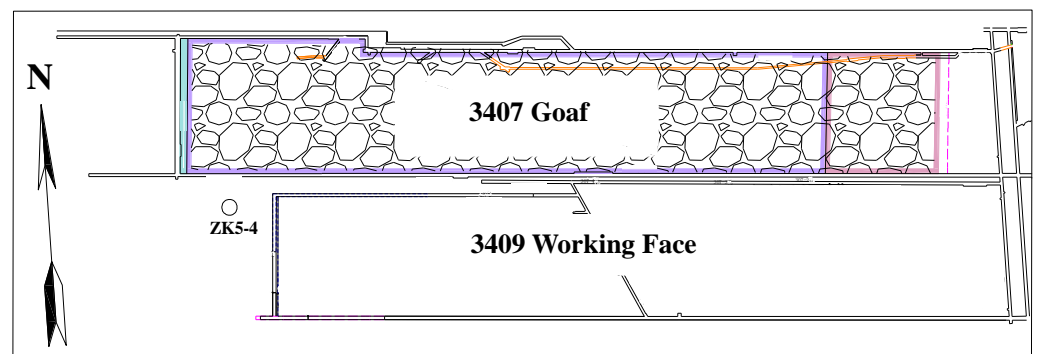


Figure 16. Layout plan of the 3409 working face in the Tingnan coal mine.

Regarding the coal pillars of the 3409 working face, a scheme of energy released and load reduction for rock burst prevention and control was proposed and applied onsite, including blasting to break the roof and coal seam drilling for pressure relief.

5.1. Energy Release Scheme for Roof Blasting

Based on the ZK5-4 borehole stratigraphy (Figures 16 and 17), multiple thick sandstone layers were present within 30 m above the coal seam, and a coarse-grained sandstone layer containing gravel, approximately 11.63 m thick, was located 70 m above the coal seam. These thick sandstone layers with high strength were key strata in the overlying rock movement and were identified as the target layers for roof blasting (Figure 17). Considering the dynamic instability mechanism under the combined effects of dynamic and static loads, roof blasting holes were constructed in the roof of the return airway, with the parameters shown in Table 3 and Figure 18.

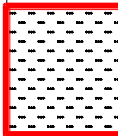

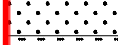



Columnar	Layer Thickness (m)	Lithology	
	11.63	Coarse grained sandstone with gravel	Target Stratum
	28.60	Weak rock layers such as mudstone	
	2.10	Fine-grained sandstone	Sandstone Formation
	1.15	Fine-grained sandstone	
	3.21	Fine-grained sandstone	
	3.56	Coarse-grained sandstone	
	18.94	Weak rock layers such as mudstone	
	8.39	No.4 Coal seam	

Figure 17. Stratigraphic diagram of the ZK5-4 borehole (partial) of the 3409 working face in the Tingnan coal mine.

Table 3. Roof blasting plan of the 3409 working face in the Tingnan coal mine.

Hole Number	1#	2#	3#	4#
Hole depth/m	44	35	34	70
Elevation angle/°	47	65	73	90
Azimuth angle/°	184	184	94	
Explosive charge/kg	45	35	35	40
Explosive charge length/m	14	11	11	12

5.2. Load Reduction Scheme for Coal Mass

Before mining, large-diameter boreholes were drilled into the coal pillar within a 300 m range ahead of the working face along the return airway crosshead for pressure relief. Figure 19 shows the plan layout of the boreholes in the coal pillar area. As depicted in the figure, the pressure relief boreholes had a diameter of 153 mm and were drilled vertically along the roadway sides. The length of boreholes on the mining side were 30 m, and those on the coal pillar side were 20 m.

5.3. Control Effect Analysis

To validate the effectiveness of the above control scheme, Figure 20 presents microseismic monitoring data collected during mining through the coal pillar section (from 1 February to 30 April 2023) [27,28]. As shown in Figure 20, after implementing the aforementioned prevention and control measures, the energy of the microseismic events detected during this period remained below 10^4 J, and there were no events of energy detected exceeding 10^4 J. The energy of the microseismic events remained below the critical threshold, indicating that the energy release scheme of roof prefracture and blasting effectively reduced the dynamic load resulting from the breakage of the overlying strata.

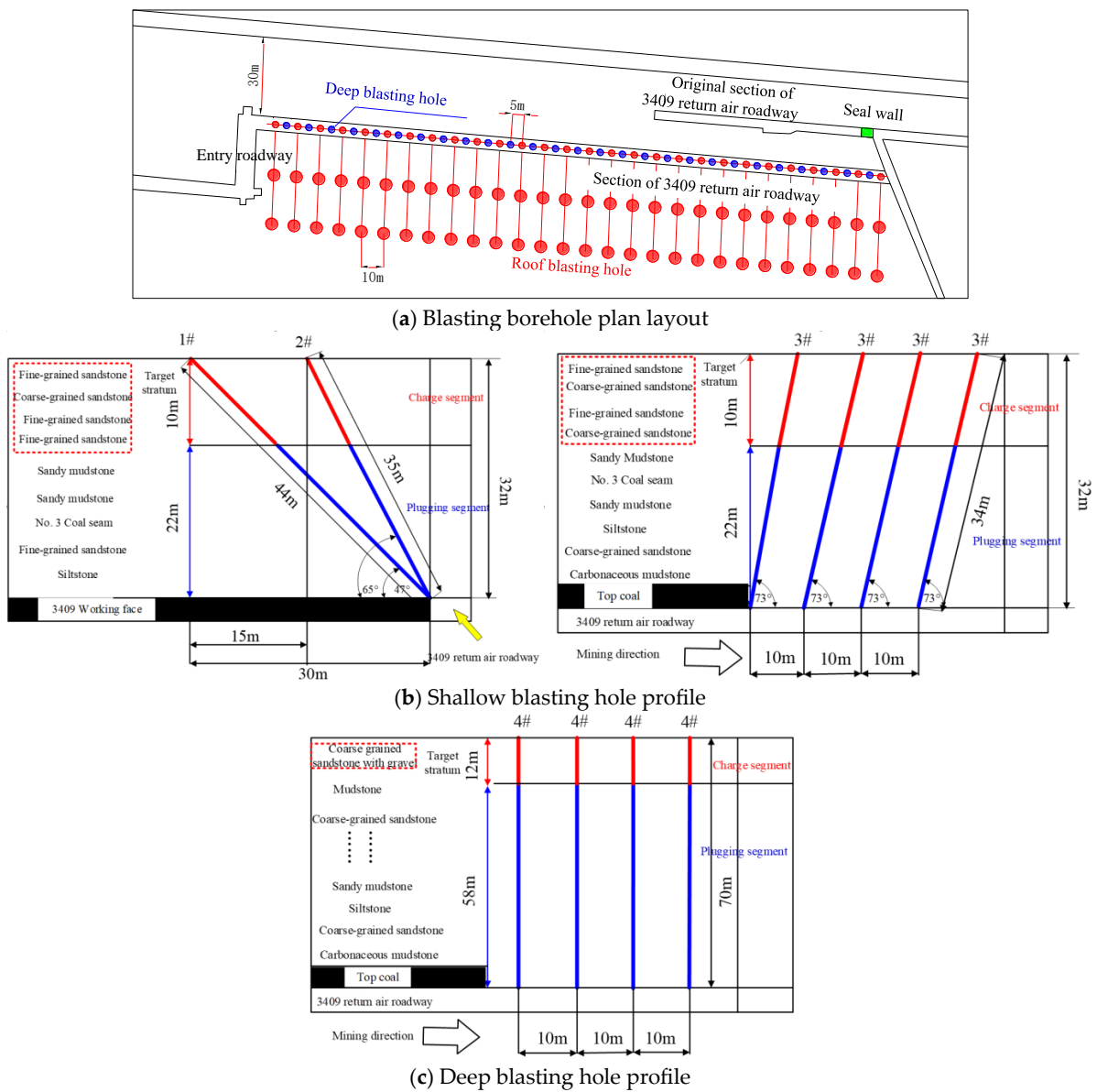


Figure 18. Layout diagram of the shallow and deep blasting holes around coal pillar of the 3409 working face in the Tingnan coal mine.

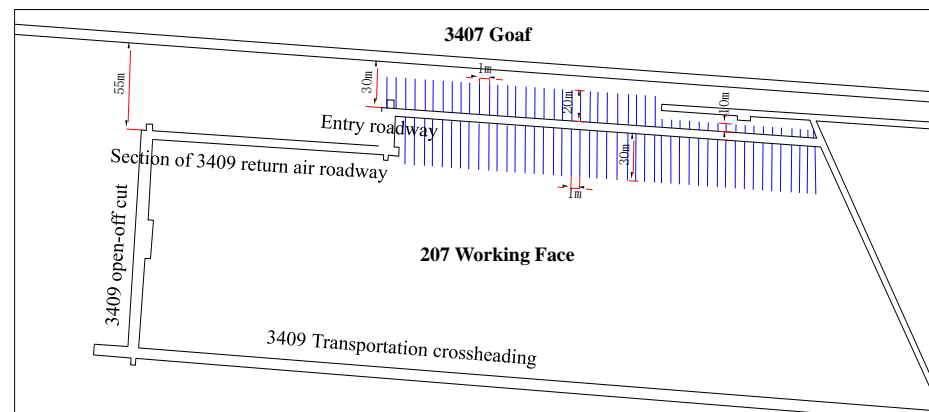


Figure 19. Schematic diagram of plane view of drilling hole around the coal pillar of the 3409 working face in the Tingnan coal mine.

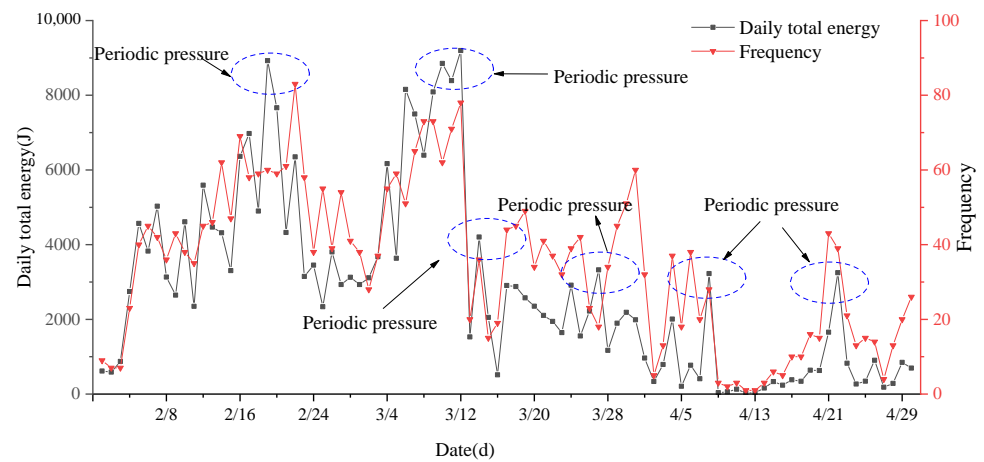


Figure 20. Microseismic monitoring data during mining around the coal pillar of the 3409 working face in the Tingnan coal mine.

Furthermore, Figure 21 presents the stress monitoring data from one set of measurement points during the transition of the coal pillar (from 1 February 2023 to 10 June 2023). As shown in the figure, when the working face passed through the coal pillar, the stress monitoring data for both the deep and shallow boreholes remained below the early warning threshold, and no sudden increases were observed. This indicates that the load reduction strategy of this high-stress coal effectively reduced the stress applied on the coal pillar. Overall, after adopting the energy release and load reduction strategy, the stress on the coal pillar and the dynamic load following the fracture of the overlying strata were effectively reduced, supporting the safe mining of this area.

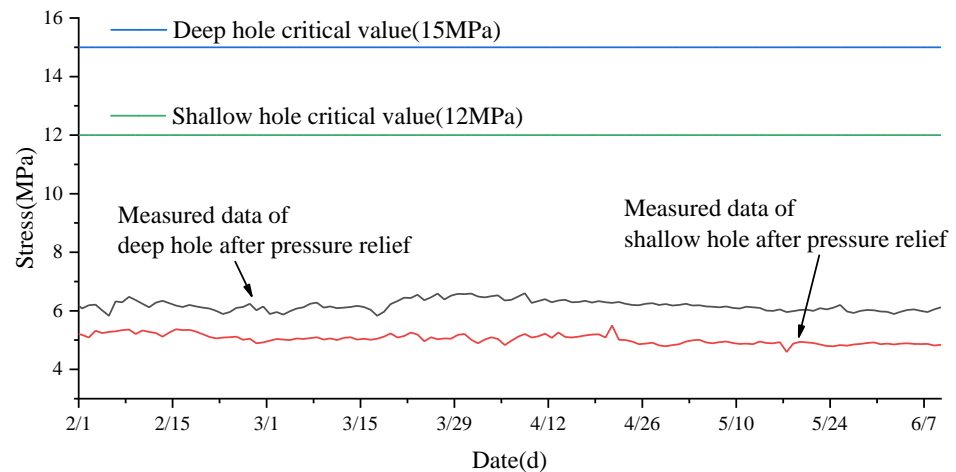


Figure 21. Stress monitoring data collected during the mining period around the coal pillar of the 3409 working face in the Tingnan coal mine.

6. Conclusions

The stress criteria for the failure of wide coal pillars under the combined effect of dynamic and static loads, as well as the energy criteria for dynamic instability, were analyzed. When the load applied on the coal pillar reaches the stress failure index for pillar failure and simultaneously satisfies the energy failure index, rock burst will occur.

The mechanical response of coal pillars under the combined effect of dynamic and static loads was investigated. With an increase in the static load, both the stress within the coal pillar and the size of the plastic zones on both sides of the coal pillar tend to increase. Under a given dynamic load, the stress and the range of the plastic zones increase significantly compared to those under conditions without a dynamic load applied.

Under a given static load, as the dynamic load increases, the coal pillar is more prone to dynamic instability.

For coal pillars with both a static load and a dynamic load caused by overburden rock fracturing, the evolution process of coal pillar dynamic instability of energy accumulation–local instability–dynamic instability was proposed. When the critical conditions for coal pillar dynamic instability in terms of stress and energy are met, rock burst will occur.

Based on the rock burst occurrence mechanism involving wide coal pillars, a rock burst prevention and control scheme of energy release and load reduction was proposed from the perspective of reducing both the static and dynamic loads on coal pillars. This scheme was implemented on the wide coal pillar area of the 3409 working face in the Tingnan coal mine, effectively reducing the threat of rock burst occurrence.

Author Contributions: Conceptualization, W.L. and B.J.; methodology, S.G.; software, Y.X.; validation, S.G.; formal analysis, Y.X. and M.D.; investigation, M.D. and W.L.; data curation, S.G.; writing—original draft preparation, Y.X. and W.L.; writing—review and editing, M.D. and B.J.; visualization, S.G.; project administration, S.G.; funding acquisition, B.J. and S.G. All authors have read and agreed to the published version of the manuscript.

Funding: This research is funded by the National Natural Science Foundation of China (52374129, 52004144) and the Natural Science Foundation of Shandong Province, China (ZR2023ME147).

Data Availability Statement: The data used to support the finding of this study are available from the corresponding author upon request.

Conflicts of Interest: The authors declare that they have no conflicts of interest regarding the publication of this work.

References

- Gu, S.; Wang, C.; Li, W.; Gui, B.; Jiang, B.; Ren, T.; Xiao, Z. Study on the technical management practice of rock burst prevention and control—Case study of Yankuang Energy Group Co., Ltd. *Geohazard Mech.* **2023**; *in press*.
- Pan, Y.S.; Song, Y.M.; Liu, J. Pattern, change and new situation of coal mine rockburst prevention and control in China. *Chin. J. Rock. Mech. Eng.* **2023**, *42*, 2081–2095.
- Li, W.S.; Jiang, B.Y.; Gu, S.T.; Yang, X.X.; Shaikh, F.U.A. Experimental study on the shear behavior of grout-infilled specimens and micromechanical properties of grout-rock interface. *J. Cent. South. Univ.* **2022**, *29*, 1686–1700. [[CrossRef](#)]
- Gong, F.Q.; He, Z.C.; Jiang, Q. Internal mechanism of reducing rock burst proneness of rock under high stress by real-time drilling pressure relief. *Rock. Mech. Rock. Eng.* **2022**, *55*, 5063–5081. [[CrossRef](#)]
- Dou, L.; Tian, X.; Cao, A.; Gong, S.; He, H.; He, J.; Cai, W.; Li, X. Current situation and difficulties in the prevention and control of coal mine burst in China. *J. Coal Ind.* **2022**, *47*, 152–171.
- Wen, Z.; Jing, S.; Song, Z.; Jiang, Y.; Tang, J.; Zhao, R.; Xiao, Q.; Zhang, T.; Wang, H.; Zhao, H.; et al. Study on coal face spatial structure model and control related dynamic disasters. *Coal Sci. Technol.* **2019**, *47*, 52–61.
- Qi, Q.; Pan, Y.; Li, H.; Jiang, D.; Shu, L.; Zhao, S.; Zhang, Y.; Pan, J.; Li, H.; Pan, P. Theoretical basis and key technologies for coal and rock dynamic disaster prevention and control in deep coal mining. *J. Coal Sci.* **2020**, *45*, 1567–1584.
- Wojtecki, L.; Goda, I. A Comparison of the seismic effects of different blasting types executed during the longwall mining of a coal seam. *J. Min. Sci.* **2020**, *56*, 947–961. [[CrossRef](#)]
- Li, W.; Jiang, B.; Li, Z.; Wang, L.; Yang, X. Strength and failure characteristics of coal measures mudstone specimens containing a prefabricated flaw under true triaxial tests. *J. Cent. South. Univ.* **2024**, *31*, 196–209. [[CrossRef](#)]
- Andrieux, P.; Hadjigeorgiou, J. The destressability index methodology for the assessment of the likelihood of success of a large-scale confined destress blast in an underground mine pillar. *Int. J. Rock. Mech. Min. Sci.* **2008**, *45*, 407–421. [[CrossRef](#)]
- Bruce, H.; Jim, G. A review of the geomechanics aspects of a double fatality coal burst at Austar Colliery in NSW, Australia in April 2014. *Int. J. Min. Sci. Technol.* **2017**, *27*, 3–7.
- Konicek, P.; Soucek, K.; Stas, L.; Singh, R. Long-hole destress blasting for rockburst control during deep underground coal mining. *Int. J. Rock. Mech. Min.* **2013**, *61*, 141–153. [[CrossRef](#)]
- Yu, X.; Wang, Q.; Zhao, B.; Bo, Q.; Wang, H. Research on the reasonable width of coal pillars between roadways in large mining height double lane arrangement working face. *J. Rock. Mech. Eng.* **2015**, *34*, 3328–3336.
- Zhang, G.; He, F. Asymmetric failure mechanism and control measures of the roof of the fully mechanized top coal caving roadway under large cross-section strong mining. *J. Rock. Mech. Eng.* **2016**, *35*, 806–818.
- Wang, H. *Research on the Creep Characteristics and Stability Control Technology of Narrow Side of Gob Tunnel*; China University of Science and Technology: Xuzhou, China, 2011.

16. Zhang, J.; Song, Z.; Liu, J.; Dong, X.; Zhang, Y.; Qi, Q.; Zhao, S.; Qin, K.; Chen, J.; Yan, T. Technical framework for structural control of rock burst disasters in deep coal mining. *Coal Sci. Technol.* **2022**, *50*, 27–36.
17. Nian, J.; Zhao, B.; Zhang, W. Numerical simulation research on the pressure relief and permeability enhancement mechanism of large-diameter borehole in coal seam. *Geofluids* **2022**, *2022*, 2926213. [[CrossRef](#)]
18. Kan, J.L.; Dou, L.M.; Li, X.W.; Li, J.Z.; Chai, Y.J. Investigating the destressing mechanism of roof deep-hole blasting for mitigating rock bursts in underground coal mines. *Geomat. Nat. Hazards Risk* **2022**, *13*, 2508–2534. [[CrossRef](#)]
19. Singh, R.; Singh, A.K.; Maiti, J.; Mandal, P.K.; Singh, R.; Kumar, R. An observational approach for assessment of dynamic loading during underground coal pillar extraction. *Int. J. Rock. Mech. Min.* **2011**, *48*, 794–804. [[CrossRef](#)]
20. Dou, L.; Bai, J.; Li, X.; He, H. Research on the prevention and control technology of rock burst disasters based on the principle of dynamic and static load superposition. *Coal Sci. Technol.* **2018**, *46*, 1–8.
21. Dou, L.M.; Cai, W.; Cao, A.Y.; Guo, W.H. Comprehensive early warning of rock burst utilizing microseismic multi-parameter indices. *Int. J. Min. Sci. Technol.* **2018**, *28*, 767–774. [[CrossRef](#)]
22. Cai, W.; Dou, L.M.; Gong, S.Y.; Li, Z.L.; Yuan, S.S. Quantitative analysis of seismic velocity tomography in rock burst hazard assessment. *Nat. Hazards* **2015**, *75*, 2453–2465. [[CrossRef](#)]
23. Wang, G.; Zhu, S.; Jiang, F.; Zhang, X.; Liu, J.; Wang, X.; Ning, T.; Zhang, Y.; Wei, Q. Coal pillar key layer structure instability type mine earthquake mechanism in inclined thick coal seam fully mechanized caving working face. *J. Coal Sci.* **2022**, *47*, 2289–2299.
24. Zhang, M.; Jiang, F.; Li, K.; Wang, C.; Wu, X.; Gao, H.; Ji, S. Research on coordinated deformation and stability of thick rock strata coal pillar system. *J. Rock. Mech. Eng.* **2017**, *36*, 326–334.
25. Wang, T.; You, S.; Pei, F.; Bai, X. Instability mechanism and prevention technology of free coal pillar under hard roof condition. *J. Min. Saf. Eng.* **2017**, *34*, 54–59.
26. Guo, W.; Deng, K.; Zou, Y. Theoretical study on catastrophic failure and instability of striped coal pillars. *J. China Univ. Min. Technol.* **2005**, *1*, 80–84.
27. Fulawka, K.; Mertuszka, P.; Pytel, W.; Szumny, M.; Jones, T. Seismic evaluation of the distress blasting efficiency. *J. Rock. Mech. Geotech. Eng.* **2022**, *14*, 1501–1513. [[CrossRef](#)]
28. Hosseini, N. Evaluation of the rockburst potential in longwall coal mining using passive seismic velocity tomography and image subtraction technique. *J. Seism.* **2017**, *21*, 1101–1110. [[CrossRef](#)]

Disclaimer/Publisher’s Note: The statements, opinions and data contained in all publications are solely those of the individual author(s) and contributor(s) and not of MDPI and/or the editor(s). MDPI and/or the editor(s) disclaim responsibility for any injury to people or property resulting from any ideas, methods, instructions or products referred to in the content.